

Solution-Processable Hole-Generation Layer and Electron-Transporting Layer: Towards High-Performance, Alternating-Current-Driven, Field-Induced Polymer Electroluminescent Devices

Yonghua Chen, Yingdong Xia, Gregory M. Smith, Hengda Sun, Dezhi Yang, Dongge Ma,* Yuan Li, Wenxiao Huang, and David L. Carroll*

The effect of solution-processed p-type doping of hole-generation layers (HGLs) and electron-transporting layer (ETLs) are systematically investigated on the performance of solution-processable alternating current (AC) field-induced polymer EL (FIPEL) devices in terms of hole-generation capability of HGLs and electron-transporting characteristics of ETLs. A variety of p-type doping conjugated polymers and a series of solution-processed electron-transporting small molecules are employed. It is found that the free hole density in p-type doping HGLs and electron mobility of solution-processed ETLs are directly related to the device performance, and that the hole-transporting characteristics of ETLs also play an important role since holes need to be injected from electrode through ETLs to refill the depleted HGLs in the positive half of the AC cycle. As a result, the best FIPEL device exhibits exceptional performance: a low turn-on voltage of 12 V, a maximum luminance of 20 500 cd m⁻², a maximum current and power efficiency of 110.7 cd A⁻¹ and 29.3 lm W⁻¹. To the best of the authors' knowledge, this is the highest report to date among FIPEL devices driven by AC voltage.

1. Introduction

Organic thin-film electroluminescent (EL) devices have drawn increasing attention due to their application full-color flexible displays and solid-state lighting.^[1–8] In particular, organic light-emitting diodes (OLEDs) have been attracting much attention because of their low cost, high contrast, fast switching speed,

and wide viewing angle.^[1,2,4] However, OLEDs typically operate with direct current (DC) voltage, which requires power converters (introducing power losses). Furthermore, light emitting diodes are typically sensitive to dimensional variations that can lead to run away currents at imperfections when large area emitting surfaces are required. A potential solution for this problem has been introduced recently that stimulates light emission from an organic emitter directly from a time dependent electric field, and little if any direct current injection from the contacts is present. This “field induced electroluminescence” approach places the emitter between two capacitor plates—one of which is transparent—with a dielectric layer to prevent direct current flow.^[9–23] The configuration is driven by an alternating current (AC) power supply, and the inorganic/organic emitter is being

stimulated primarily by an induced polarization current within the capacitor. While much work is still needed to understand if AC-driven EL devices might offer an alternative to standard OLED technologies, it seems reasonable to assert that competitive manufacturing advantage would arise from such devices if they could be shown to be bright and efficient.

Inorganic EL devices driven by AC have previously been well established, which consist of a polycrystalline phosphor layer doped with a luminescent impurity (e.g., Mn or Cu) that is enclosed between a pair of insulating layers.^[9,10] Unlike these inorganic devices, AC field-induced EL devices based on organic molecules or conductive polymers can have high quantum efficiencies arising from the radiative decay of excitons and they are easy to fabricate using vacuum deposition or solution processes under ambient conditions.^[11,12] The first such AC field-induced organic EL device was reported in 2000,^[11] where the blue emission EL mechanism was proposed to be through impact excitation of organic molecules after bombardment with hot electrons accelerated through the dielectric layers.

More recently, there have been efforts to fabricate AC field-induced organic EL devices, wherein charge carriers are

Dr. Y. Chen, Dr. Y. Xia, G. M. Smith, Dr Y. Li, W. Huang, Prof. D. L. Carroll
Center for Nanotechnology and Molecular Materials
Department of Physics
Wake Forest University
Winston-Salem, NC, 27105, USA
E-mail: carrolldl@wfu.edu



H. Sun, Dr. D. Yang, Prof. D. Ma
State Key Laboratory of Polymer Physics and Chemistry
Changchun Institute of Applied Chemistry
Chinese Academy of Sciences
Changchun, 130022, P. R. China
E-mail: mdg1014@ciac.jl.cn

DOI: 10.1002/adfm.201303242

generated within the organic layers external to the emitter, or allowed to originate from external electrodes.^[13–23] In both cases light generation is achieved through the AC field-induced creation of excitons-bipolar charges generated and injected from internal charge generation layers or simply injected directly from an electrode (similar to OLEDs) with the subsequent recombination of these holes and electrons in the emissive layer (EML). An example of bipolar charges injected directly from electrodes has been given by using single-walled carbon nanotubes (SWNTs) or multi-walled carbon nanotubes (MWNTs) as channels for transport of holes and electrons.^[16,18] In this work a maximum luminance of approximately 350 and 100 cd m⁻² were achieved. Likewise, a representative example for charge-carrier generation within the device without injecting charge carriers is a recent work employing the concept of molecular doping for small molecule organic semiconductors, allowing for efficient transport as well as for generation of charge carriers.^[13–15,17,23] A small-molecule red phosphorescent emission with luminance up to 1500 cd m⁻² and 5000 cd m⁻² (with optical design) was observed when the device is driven with an AC voltage. These two examples demonstrate the potential flexibility in fabrication and design of such devices, suggesting fields of application from multicolor display devices to white large-area lighting panels might be possible. Moreover, AC driven EL devices are potentially stable because they avoid the charge accumulation in the device due to frequent reversal of the applied voltage.^[13] The dielectric layer can also effectively prevent electro-chemical reactions between the organic layer and the electrodes and protecting from degradation due to external moisture and oxygen in the atmosphere.^[16] Challenges remain, however, in terms of the high voltage, low luminance, and low efficiency.

We previously reported a facile method to improve the performance in a solution-processable AC-driven organic EL device.^[21] The key feature of our strategy is employing a solution processable high-*k* polymer as dielectric layer to lower the driven voltage and a combination of a solution-processable p-doped hole-generation layer (HGL) with a solution-processable high-triplet and high-electron-mobility material as the electron-transporting layer (ETL) to effectively create excitons. The excitons are formed by the generated holes from HGL and the injected electrons from ETL. As a result, the devices have maximum luminance values of 13 800 cd m⁻² without any outcoupling technology and optical design under an AC voltage driven.

In this paper, motivated by the fact that the light generated in our devices is due to the recombination of injection of electrons and generation of holes under AC driven voltage, the effect of solution-processed HGL and ETL are systematically investigated on the performance of solution-processable AC field-induced polymer EL (FIPEL) devices in terms of hole-generation capability of HGL and electron-transporting characteristics of ETL. We investigate p-type doping of a variety of conjugated polymers with a wide range of the highest occupied molecular orbital (HOMO) levels by tetrafluoro-tetracyanoquinodimethane (F4TCNQ) via solution-processed co-blending and electron-transporting characteristics of a series of solution-processed electron-transporting small molecules. Regardless of the dielectric layer, we found that the free hole density and conductivity in p-doped HGL and electron mobility in

solution-processed ETL are directly related to the device performance. As a result, we have fabricated green FIPEL devices with exceptional performance: a low turn-on voltage of 12 V, a maximum luminance of 20 500 cd m⁻², a maximum current efficiency and power efficiency of 110.7 cd A⁻¹ and 29.3 lm W⁻¹. To the best of our knowledge, this is the highest report to date among FIPEL devices driven by AC voltage.

2. Results and Discussions

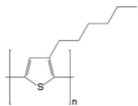
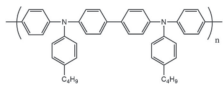
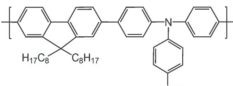
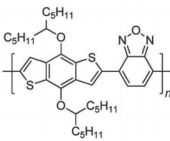
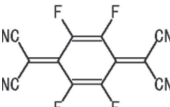
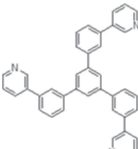
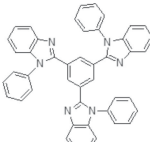
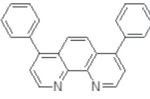
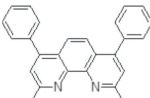
2.1. Hole-Generation Capability of p-Doped Conjugated Polymers by F4TCNQ

The p-type conjugated polymers we used include poly(3-hexylthiophene) (P3HT), poly(*N,N'*-bis(4-butylphenyl)-*N,N'*-bis(phenyl) benzidine) (Poly-TPD), poly(9,9-di-*n*-octylfluorene-*alt*-(1,4-phenylene-((4-*sec*-butylphenyl) imino)-1,4-phenylene) (TFB), and poly[4,8-bis(1-pentylhexyl)benzo[1,2-*b*:4,5-*b'*]dithiophene-2,6-diyl-*alt*-2,1,3-benzoxadiazole-4,7-diyl] (P1).^[24] Their chemical structures and optoelectronic properties are summarized in Table 1. The HOMO levels of these polymers ranges from 5.1 eV (P3HT)^[25] to 5.34 eV (P1).^[24] The concentration of F4TCNQ in polymers solutions is fixed at 7% (by weight). The doped solutions were clear with no precipitation, which allows for convenient solution processing through spin-coating to fabricate thin films.

In fact, the basic principle of p-type doping in organic semiconductors is equivalent to that in inorganic materials. Free holes can be introduced into the semiconductor by the charge transfer from the HOMO levels of polymer to the lowest unoccupied molecular orbital (LUMO) levels of F4TCNQ acceptor due to exceptionally strong acceptor character of F4TCNQ molecules.^[26] This leads to a gradual shift of the polymer Fermi level towards its HOMO level, which effectively reduces the interface potential barrier. Therefore, hole-only (HO) devices were constructed to study the effect of p-type doping by F4TCNQ on the transport properties of polymers, from which hole mobility and free hole density were subsequently deduced.^[27] A series of hole-only devices with structure of ITO/PEDOT (40 nm)/polymers:F4TCNQ (≈150 nm)/MoO₃ (5 nm)/Al are fabricated. ITO is positive and Al is negative. The thin MoO₃ layers at the side of Al electrode is used for blocking the electron injection. The *J*–*V* characteristics of these devices are shown in Figure 1 in double-logarithmic representation.

Due to the close HOMO levels between PEDOT:PSS (5.2 eV) and polymers (Table 1), the hole-injection barrier at the PEDOT:PSS/polymer interface can be negligible. At 7% F4TCNQ doping, P3HT shows the highest hole-current at all voltages with a linear *J*–*V* characteristic compared to other polymers. This suggests a substantial increase in bulk conductivity via F4TCNQ doping to metallic-like conduction, which is consistent with its highest field-effect hole mobility measured by time-of-flight or FETs.^[28] Poly-TPD shows marginally higher hole-current than that of TFB. In both cases, there is a sharp turn-on at 0.6 V, suggesting contact-limited hole-injection at low voltages. P1 with a deeper HOMO level exhibits the lowest hole current, which corresponds to the low short circuit current in organic solar cells.^[24]

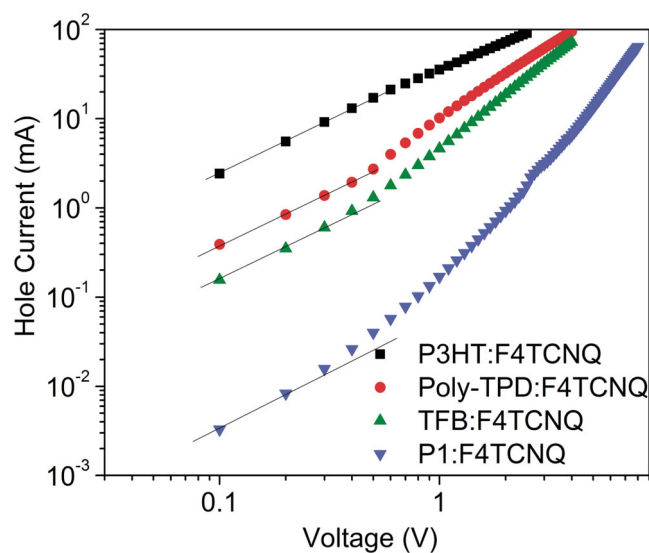
Table 1. Chemical structures and optoelectronic properties of solution-processable conjugated polymer and small molecules.

Materials	Chemical Structure	LUMO	HOMO
P3HT		3.2	5.1
Poly-TPD		2.3	5.2
TFB		2.1	5.3
P1		3.45	5.34
F4TCNQ		5.2	8.3
TmPyPB		2.8	6.7
TPBi		2.7	6.2
Bphen		2.6	6.0
BCP		3.2	6.7

At low voltages, the hole mobility is constant at room temperature,^[29] and the J - V characteristics follow Child's law given by,^[30]

$$J_{\text{SCLC}} = \frac{9}{8} \epsilon_0 \epsilon_r \mu_p \frac{V^2}{d^3} \quad (1)$$

Where ϵ_0 is the permittivity of free space, ϵ is the relative permittivity, μ_p is the zero-field hole mobility, and d is the thickness of the polymer layer. From the slope of the $\log J$ - $\log V$ plot of the HO device shown in Figure 1, a clear quadratic dependence of current on applied voltage is observed. Upon doping, a

**Figure 1.** Current-voltage characteristics of HO devices for p-doping polymers. The solid lines with slope of 1 denote the Ohmic contact.

clear Ohmic behavior (slope ≈ 1) at low voltage is observed in all HO devices.

Upon p-type doping free holes are introduced into the semiconductor. At low voltages these additional free holes are largely outnumber the charges that are injected from the contacts. Since the positive charge of this background density p_0 is compensated by the negative charge of the corresponding acceptors, and therefore does not contribute to the built-up of space charge, an Ohmic-like current will flow at low voltages, given by^[30]

$$J_{\Omega} = qp_0\mu_p \frac{V}{d} \quad (2)$$

where q is the magnitude of electron charge, p_0 the free hole density, μ_p the hole mobility at low voltage, and d is the thickness of the polymer layer. For increasing voltages more and more charges will be injected from the contacts and space charge starts to accumulate in the semiconductor. At a certain voltage the amount of background charge from the dopant will be equal to the injected space charge. Therefore, we can easily get the hole mobility and free hole density of the p-doped polymer.

Table 2 summarizes the transport properties of the p-doped polymers. It can be seen that P3HT:F4TCNQ, Poly-TPD:F4TCNQ, and TFB:F4TCNQ give the maximum free hole density of $3.68 \times 10^{22} \text{ m}^{-3}$, $2.35 \times 10^{22} \text{ m}^{-3}$, and $1.52 \times 10^{22} \text{ m}^{-3}$ respectively, while only $3.01 \times 10^{21} \text{ m}^{-3}$ free hole density is created in P1:F4TCNQ HGL. Since free holes are generated by the charge transfer from the HOMO levels of polymer to the LUMO level of F4TCNQ, this can be understood in terms of their different electronic properties, i.e., P3HT, Poly-TPD, and TFB having a smaller HOMO level than that of P1 (5.1 eV,^[25] 5.2 eV,^[31] and 5.3 eV^[32] versus 5.34 eV^[24]) can undergo p-doping more easily by F4TCNQ (5.2 eV),^[26] thereby increasing the free hole density. Furthermore, the hole mobility of p-doped polymer are also investigated. It is greatly necessary that the generated

Table 2. Free hole density and hole mobility of p-doping conjugated polymer by F4TCNQ.

Properties	P3HT:F4TCNQ	Poly-TPD:F4TCNQ	TFB:F4TCNQ	P1:F4TCNQ
Free hole density (m^{-3})	3.68×10^{22}	2.35×10^{22}	1.52×10^{22}	3.01×10^{21}
Hole mobility ($\text{cm}^2 \text{V}^{-1} \text{s}^{-1}$)	6.7×10^{-4}	2.4×10^{-4}	1.7×10^{-4}	3.0×10^{-5}

charges must rapidly transport into the EML. Otherwise, it could cause large voltage drop and even quench the generated charges by the space electrical field induced by the charge accumulation.^[33] The hole mobility are $6.7 \times 10^{-4} \text{ cm}^2 \text{V}^{-1} \text{s}^{-1}$ for P3HT:F4TCNQ, $2.4 \times 10^{-4} \text{ cm}^2 \text{V}^{-1} \text{s}^{-1}$ Poly-TPD:F4TCNQ, $1.7 \times 10^{-4} \text{ cm}^2 \text{V}^{-1} \text{s}^{-1}$ for TFB:F4TCNQ, and $3.0 \times 10^{-5} \text{ cm}^2 \text{V}^{-1} \text{s}^{-1}$ for P1:F4TCNQ. The high free hole density and hole mobility could in principle lead to high luminance in our FIPEL devices.

2.2. Electron-Transporting Characteristics of Solution-Processed ETLs.

The commercial electron-transport materials, 1,3,5-tri(m-pyrid-3-yl-phenyl)benzene (TmPyPB), 1,3,5-Tri(1-phenyl-1H-benzod[imidazol-2-yl]phenyl) (TPBi), 4,7-diphenyl-1,10-phenanthroline (Bphen), and bathocuproine (BCP) were employed. Their chemical structures and optoelectronic properties are also summarized in Table 1. Due to the solvent used to deposit the subsequent layer tends to dissolve the underlying layer, our strategy towards overcoming this problem is to utilize formic acid:water (FA:H₂O = 3:1) mixture as solvent for the electron-transport materials as previous reports.^[34–37]

The ETL in our device design is also important regarding to the electron mobility and energy level. Although the electron mobility of small-molecule electron-transporting materials by vacuum evaporation has widely been investigated,^[38] the remarkable observation that needs to be addressed is the electron mobility of these materials by solution process. Therefore, electron-only (EO) devices were constructed to study the transport properties of solution-processed small molecules, from which electron mobility were subsequently deduced. A series of electron-only devices with structure of ITO/TiO_x (20 nm)/TmPyPB, TPBi, Bphen, or BCP (≈ 150 nm)/LiF (1 nm)/Al are fabricated. ITO is positive and Al is negative. The TiO_x layers at the side of ITO electrode is used for blocking the hole injection. The J - V characteristics of these devices are shown in Figure 2 in double-logarithmic representation.

The electron mobility was extracted by fitting the J - V curves in the near quadratic region, the current density is given by,^[39]

$$J = \frac{9}{8} \epsilon \epsilon_0 \mu_e \frac{V^2}{d^3} \exp\left(0.89\beta \frac{\sqrt{V}}{\sqrt{d}}\right) \quad (3)$$

where J is the current density, ϵ_0 is the permittivity of free space, ϵ is the relative permittivity, μ_e is the zero-field mobility, V is the applied voltage, d is the thickness of active layer, and b is the field-activation factor. The solid lines in Figure 2 represent the SCLC fitting curves in the quadratic SCLC region. The SCLC fitting curve matches well with the measured J - V curve, since all the adjusted R-squared values from the curve-fitting

were higher than 0.99, which demonstrates a good quality of the fits. The electron mobility estimated from these devices for TmPyPB, TPBi, Bphen, and BCP are 7.0×10^{-7} , 3.2×10^{-7} , 2.2×10^{-6} , and 7.7×10^{-8} , respectively (Table 3), which corresponds to the previous reports.^[37] The high-performance FIPEL devices could achieve using ETLs with high electron mobility since electrons can be transported in a low voltage.

2.3. Fabrication and Characterization of the AC-Driven FIPEL Devices

Figure 3 shows a schematic illustration (Figure 3a) and the corresponding energy level diagram and proposed charge carriers recombination process (Figure 3b) of the AC-driven FIPEL device structures. A dielectric layer of poly(vinylidene fluoride-trifluoroethylene-chlorofluoroethylene) [P(VDF-TrFE-CFE)], which shows high dielectric constant as our previous report,^[21] is placed against the bottom ITO electrode and the EML is sandwiched between a HGL and a ETL. In order to obtain the high-performance FIPEL devices, we used high-efficiency metallo-organic phosphores, fac-tris(2-phenylpyridine)iridium(III) [Ir(ppy)₃] for green emission,^[40] which can harvest both singlet and triplet excitons. 10% Ir(ppy)₃ by weight are doped into a co-host of blending poly(*N*-vinylcarbazole) (PVK) and 1,3-bis(2-(4-*tert*-butylphenyl)-1,3,4-oxadiazol-5-yl)benzene (OXD-7) (PVK:OXD-7 = 8:2) as the EML.^[41–44]

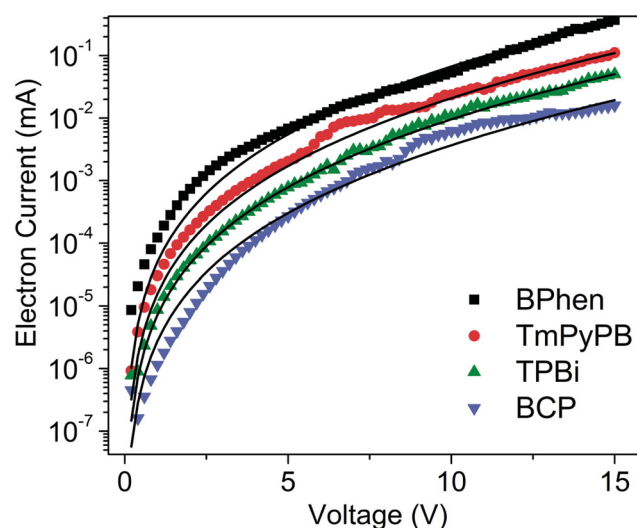


Figure 2. Current–voltage characteristics of EO devices for solution-processed small molecules. The solid lines represent the SCLC model with field-dependent mobility.

Table 3. Electron mobility of solution-processable small molecules.

Properties	TmPyPB	TPBi	Bphen	BCP
Electron mobility ($\text{cm}^2 \text{V}^{-1} \text{s}^{-1}$)	7.0×10^{-7}	3.2×10^{-7}	2.2×10^{-6}	7.7×10^{-8}

Figure 4 shows the AC current density-voltage (J - V) characteristics of the optimized FIPEL devices with P3HT:F4TCNQ, Poly-TPD:F4TCNQ, TFB:F4TCNQ, and P1:F4TCNQ as the HGLs and TmPyPB, TPBi, Bphen, and BCP as the ETLs. All of the device performances in detail are summarized in **Table 4**. The current density was gradually increased with increasing the driven voltage in all devices, demonstrating that more holes are generated in the HGLs and more electrons are injected through the ETLs in the high voltages. The TmPyPB-based devices exhibit higher current density in the same voltages while the TPBi, Bphen, and BCP-based devices show the lower

current density. Moreover, the maximum current is achieved in the lowest voltage in P3HT:F4TCNQ HGL-based devices compared to other HGLs with the same ETL, indicating more free holes are generated and injected into the EML as demonstrated above. This can significantly enhance the luminance of the device, as shown in **Figure 5**, which displays the luminance characteristics as a function of driven voltage (L - V) characteristics of FIPEL devices. The P3HT:F4TCNQ devices give the lowest turn-on voltage (defined at 1 cd m^{-2}) of 12 V using TmPyPB as the ETL while 22 V, 23 V, and 30 V are necessary in Poly-TPD:F4TCNQ, TFB:F4TCNQ, and P1:F4TCNQ devices, respectively. The low turn-on voltage can be attributed to the high dielectric constant of P(VDF-TrFE-CFE) and high hole density and hole mobility in P3HT:F4TCNQ HGL. The turn-on voltage for onset of luminance for the P3HT:F4TCNQ device is reduced by approximately 18 V with respect to P1:F4TCNQ device using the same ETL. Furthermore, the turn-on voltage is even higher up to 36 V in the device combining

P1:F4TCNQ HGL with BCP ETL. The driven voltages are also remarkably different. For example, at the luminance of 1000 cd m^{-2} , the P3HT:F4TCNQ device shows the lowest voltage of 53 V while Poly-TPD:F4TCNQ, TFB:F4TCNQ, and P1:F4TCNQ devices give 66 V, 78 V, and 90 V in the same TmPyPB ETL. This obviously suggests that the two functional layers, HGL and ETL, are very important in the device operation regardless of the dielectric layer. This can be reasonably understood due to the fact that the excitons are formed by the combination of the generated holes from HGLs and the injected electrons through ETLs (**Figure 1b**). Accordingly, the device combining P3HT:F4TCNQ HGL with TmPyPB ETL exhibits the maximum luminance of $20\,500 \text{ cd m}^{-2}$. To the best of our knowledge, this is the highest value up to now in the reported literatures based on AC-driven devices. In the same structure, Poly-TPD:F4TCNQ, TFB:F4TCNQ, and P1:F4TCNQ devices respectively give their maximum luminance of $15\,180 \text{ cd m}^{-2}$, $10\,000 \text{ cd m}^{-2}$, and 6020 cd m^{-2} in the same TmPyPB ETL (**Table 2**). This further demonstrates that our design of combination of HGL with ETL for FIPEL device is highly efficient. The luminance of P3HT:F4TCNQ device is more than 3 times that of P1:F4TCNQ devices, which demonstrates again that the important role of HGL in our device design. Moreover, the luminance in the TmPyPB-based devices is higher than those in the TPBi, Bphen, and BCP-based devices in the same HGL. For example, in the P3HT:F4TCNQ devices, the TmPyPB, TPBi, Bphen, and BCP-based devices show the maximum luminance of $20\,500 \text{ cd m}^{-2}$, $18\,640 \text{ cd m}^{-2}$, $15\,150 \text{ cd m}^{-2}$, $10\,980 \text{ cd m}^{-2}$,

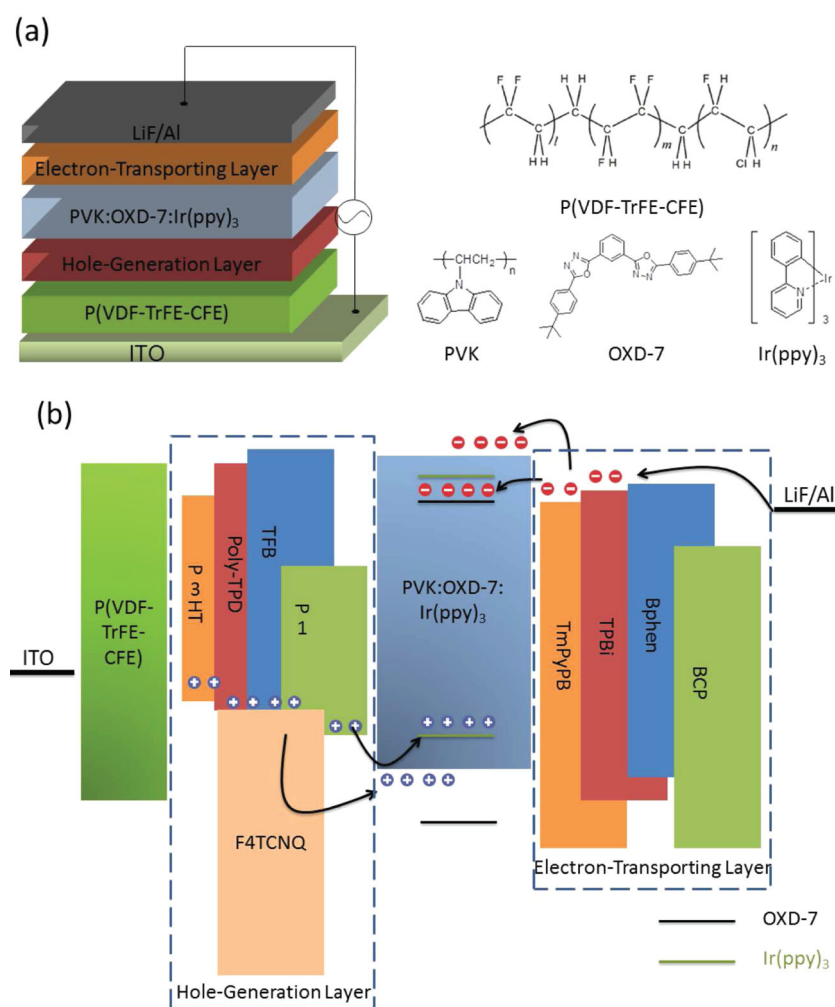


Figure 3. a) Schematic architecture of the FIPEL devices. The device structure is: ITO/P(VDF-TrFE-CFE) (1,000 nm)/HGL/PVK:OXD-7 (80:20):Ir(ppy)₃ (10 wt%) (150 nm)/ETL (40 nm)/LiF (1 nm)/Al (150 nm). The molecular structures of materials used in this study are also shown. b) Schematic energy-level diagram for the layers of the optimized FIPEL devices and the proposed hole generation and electron injection processes.

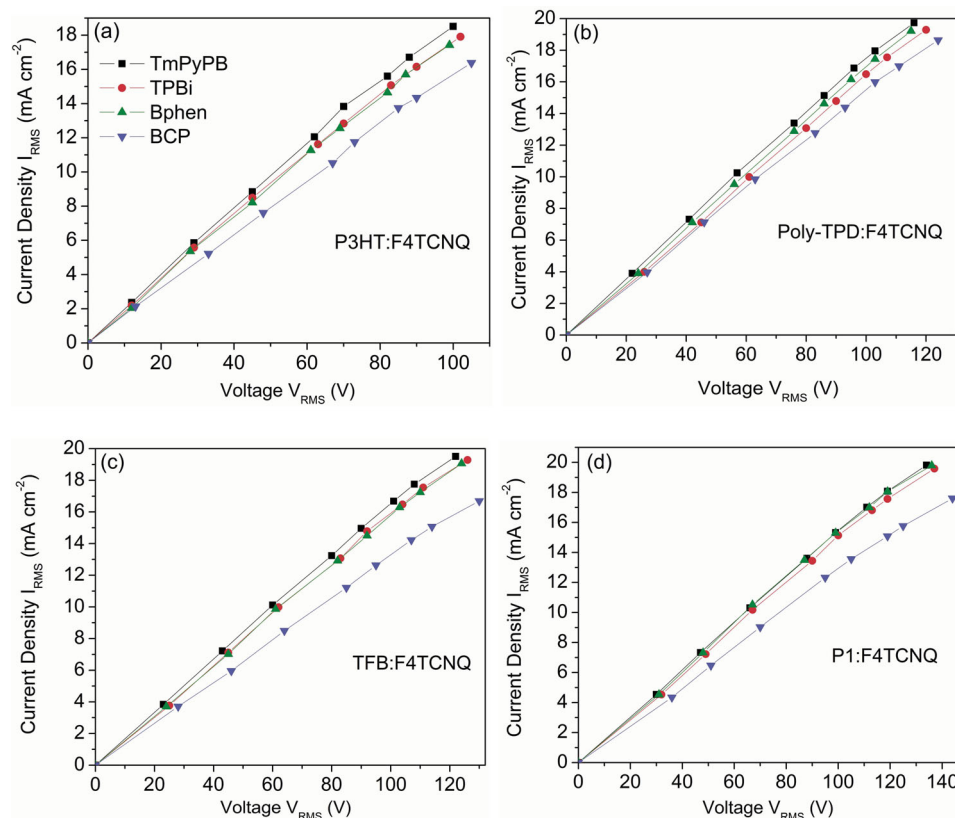


Figure 4. The AC current density-voltage characteristics of FIPEL devices with the combination of different HGLs and different ETLs.

respectively (Table 2). The luminance of TmPyPB-based device is almost 2 times higher than that of BCP-based device, which also suggests that the ETL in our device design is the other key.

This trend matches well with the observed highest FIPEL performance compared to other devices with a TmPyPB ETL except for Bphen devices. In general, FIPEL devices with high electron

Table 4. Summary of the performance of the FIPEL devices with different HGLs and ETLs.

HGLs	ETLs	$V_t^{a)}$ [V]	$L_{max}^{b)}$ [cd m ⁻²]	$\eta_{cd,max}^{c)}$ [cd A ⁻¹]	$\eta_{p,max}^{d)}$ [lm W ⁻¹]
P3HT:F4TCNQ	TmPyPB	12	20 500	110.7	29.3
	TPBi	12	18 640	104.0	27
	Bphen	12	15 150	87.0	23.2
	BCP	13	10 980	67.0	16.9
P-TPD:F4TCNQ	TmPyPB	22	15 180	76.9	16.7
	TPBi	26	13 800	71.5	15
	Bphen	24	11 400	59.3	13
	BCP	27	8770	47.1	9.5
TFB:F4TCNQ	TmPyPB	23	10 000	51.3	10.4
	TPBi	25	8260	42.8	8.4
	Bphen	24	6990	36.7	7.3
	BCP	28	5000	30.0	5.7
P1:F4TCNQ	TmPyPB	30	6020	30.4	6.3
	TPBi	32	5010	25.6	5.2
	Bphen	31	4300	21.7	4.4
	BCP	36	3000	17.0	3.3

^{a)} V_t is the turn-on voltage defined at 1 cd m⁻²; ^{b)} L_{max} is the maximum luminance; ^{c)} $\eta_{cd,max}$ is the maximum current efficiency; ^{d)} $\eta_{p,max}$ is the maximum power efficiency.

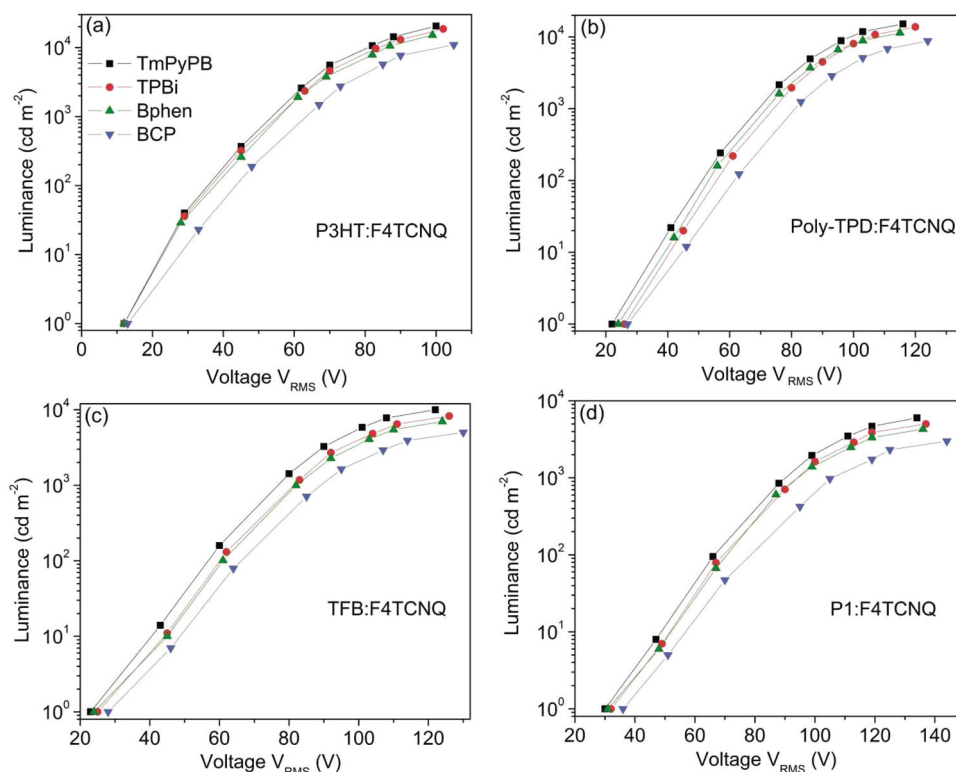


Figure 5. The luminance–voltage characteristics of FIPEL devices with the combination of different HGLs and ETLs at a fixed frequency of 60 kHz.

mobility ETLs perform better than the devices with lower electron mobility ETLs since the injected electrons can be fast transported in this layer in a low voltage. However, our results show that the FIPEL devices with solution-processed TmPyPB and TPBi ETLs showed better performance than the devices with solution-processed Bphen ETLs. Earmme et al. demonstrated that the rough surface morphology with a high density of vertically aligned nanopillars formed by strong intermolecular interactions of solution-processed Bphen ETL maximize the contact area between the ETL and Al cathode, facilitating efficient electron-injection and transport which lead to much higher device performance.^[37] According to the device operation mechanism we proposed that the emission was observed only in the negative half of the AC cycle, as shown in **Figure 6a**, however, the holes need to be injected from LiF/Al electrode through ETL as a possible responsibility for refilling the depleted HGL in the positive half of the AC cycle. The injected holes then are drift towards the insulator and neutralize the negative ionized dopants in the HGLs in the positive half of the AC cycle. This brings the system back to the original state. By this process, free holes can be regenerated that are used in the subsequent negative half of the AC cycle to generate excitons again. Therefore, the hole transporting characteristics of ETLs could play an important role in the device operation. **Figure 6b** shows the J – V characteristics of a series of hole-only devices with the device structure of ITO/PEDOT:PSS (40 nm)/PVK:OXD-7 (80:20):Ir(ppy)₃ (10 wt%) (150 nm)/ETLs (40 nm)/LiF (1 nm)/Al (150 nm), where the ITO is negative and Al is positive, in order to investigate the hole injection from LiF/Al electrode through

ETLs under DC voltages. The TmPyPB based device showed higher hole current density than TPBi, Bphen, and BCP based devices at the same voltages. Note that there is no light emission from the devices in the whole driven voltage, demonstrating no electrons injection from PEDOT:PSS. This strongly demonstrated that the holes in TmPyPB based FIPEL devices can much easier be injected into devices and refill the depleted HGL in the positive half of the AC cycle. Therefore, TmPyPB based FIPEL devices exhibit lower turn-on voltage and driven voltages. This can also be verified by the fact that, as shown in **Figure 6c**, the FIPEL device with TmPyPB ETL but without HGL exhibits higher luminance and lower voltages compared to the devices with TPBi, Bphen, and BCP ETLs. In these devices, electrons are first injected into the EML from LiF/Al electrode ETL and accumulated at the interface of P(VDF-TrFE-CFE)/EML in the negative half of the AC cycle. When the AC cycle is positive, holes are also effectively injected into the EML from LiF/Al electrode. Simultaneously, the accumulated electrons move into the EML to form excitons with the injected electrons, leading to light emission upon recombination. Therefore, the hole-transporting characteristics of ETLs also play an important role in the device operation at AC-driven condition.

The light emission from our devices is frequency dependent as we reported previously.^[13,18,21,22] The luminance characteristics as a function of frequency (L – f) characteristics for fixed AC voltage for all FIPEL devices are plotted in **Figure 7**. The luminance gradually increased and then decreased after a particular frequency for all FIPEL devices. The best frequency for luminance output from all devices is 60 kHz, which corresponds

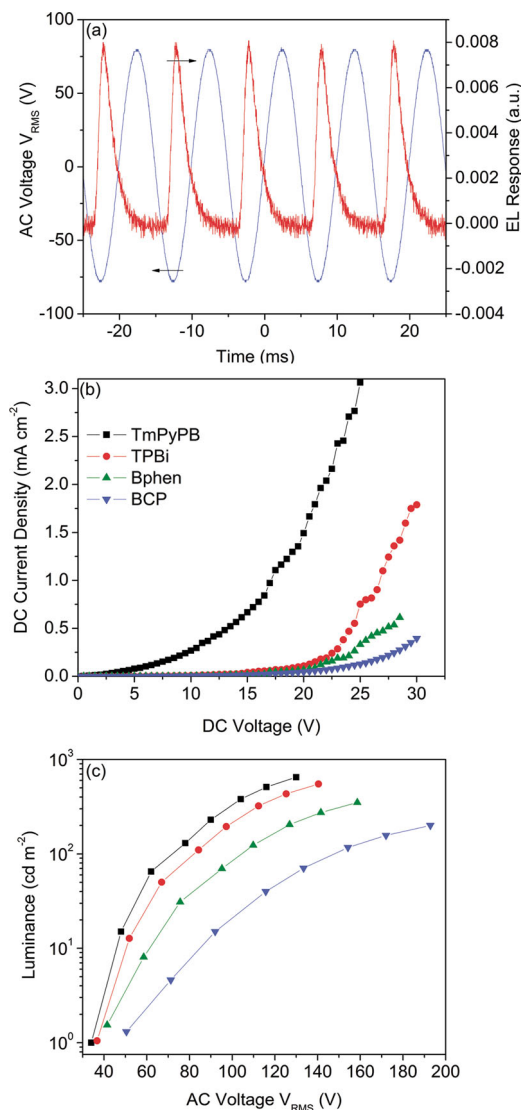


Figure 6. a) The time-resolved alternating voltage pulse at 50 Hz (left axis) and the corresponding TREL as recorded by the photodetector (right axis) for the device using P3HT:F4TCNQ as a HGL and TmPyPB as an ETL. The device emits light only in the negative half of the AC cycle. b) Current density–voltage characteristics of hole-only devices. c) Luminance–AC voltage characteristics of FIPEL devices with device structure of ITO/P(VDF-TrFE-CFE) (1,000 nm)/PVK:OXD-7 (80:20):Ir(ppy)₃ (10 wt%) (150 nm)/ETL (40 nm)/LiF (1 nm)/Al (150 nm).

to our previous report.^[21] It is important to note that the luminance tends towards zero as the frequency approaches zero, indicating clearly the capacitive nature of the device. The increase in luminance from low frequency to 60 kHz is due to the increase in current flowing through the device, as the capacitive reactance of the device is inversely proportional to the frequency.^[13,21] At high frequencies after 60 kHz, the charge carrier recombination begins to be limited by mobility in the active layer.^[13] This leads to a decrease in the luminance beyond a particular frequency, for example, 60 kHz. The charge carriers may not even be injected or the generated charge carriers could not be extracted at very high frequencies, resulting

in a reduction of the number of charge carriers available in the emissive layer, which leads to a decrease in luminance.

For a capacitive coupled AC-driven device, the phase characteristics are very important quantities. The impedance, reactance, resistance, and the phase angle as a function of operation frequency of the FIPEL device using different HGL and TmPyPB ETL as examples are shown in Figure 8. The impedance (Figure 8a) is dominated by the reactance (Figure 8b) whereas a significantly smaller contribution comes from the resistance (Figure 8c), which demonstrates that our FIPEL is typical capacitive devices. All three resistive quantities show a pronounced decrease from low (1 kHz) to high frequency (100 kHz), which correspond to the previous report. The decreased impedance and reactance with increasing frequencies further demonstrates that our FIPEL is typical capacitive devices. Moreover, the three resistive quantities are increased from P3HT:F4TCNQ to P1:F4TCNQ HGL based devices, which may be related to the free hole density and hole mobility in the HGLs. The phase angle (Figure 5d), which is the most crucial for a correct power efficiency calculation, are decreased from 89° to 80° at this range of frequency for all FIPEL devices, corresponding to our previous report. The phase angles are all around 83° at the best frequency for luminance.

Figure 9 and Figure 10 show the current (η_{cd}) and power efficiency (η_{p}) as a function of luminance of FIPEL devices, respectively. The current efficiency (η_{cd}) is defined as the ratio of luminance output from the device to the RMS current flowing the device, which is given in candela per ampere (cd A^{-1}). The power efficiency (η_{p}) is defined as the ratio of photometric power emitted from the device to the electrical input power.^[13] The maximum η_{cd} and η_{p} of 110.7 cd A^{-1} and 29.3 lm W^{-1} are achieved in P3HT:F4TCNQ device employing TmPyPB as the ETL, whereas those are 76.9 cd A^{-1} and 16.7 lm W^{-1} for Poly-TPD:F4TCNQ device, 51.3 cd A^{-1} and 10.4 lm W^{-1} for TFB:F4TCNQ device, and 30.4 cd A^{-1} and 6.3 lm W^{-1} for P1:F4TCNQ device (Table 4). The P3HT:F4TCNQ device exhibits higher efficiency due to its high luminance in low current and reduced driven voltage. The η_{cd} are comparable with or even higher than solution-processed or evaporating small-molecular OLEDs.^[45–50] The best power efficiency is even 1.7–10 times higher than the previous highest value report.^[17,21] Moreover, all devices exhibit the peak efficiencies at high luminance, which is different from OLEDs usually accompanied by efficiency roll-off at high luminance.^[51,52] For example, the η_{cd} and η_{p} for P3HT:F4TCNQ device are 16.4 cd A^{-1} and 4.5 lm W^{-1} at a luminance of 1000 cd m^{-2} , 68.3 cd A^{-1} and 22 lm W^{-1} at a luminance of 10 000 cd m^{-2} , and 110.1 cd A^{-1} and 29 lm W^{-1} at a luminance of 20 000 cd m^{-2} , respectively. This confirms again that our design concept is a predominant technique for achieving high-efficiency FIPEL devices.

3. Conclusions

The effect of solution-processed p-doped HGLs and ETLs are systematically investigated on the performance of all-solution-processable FIPEL devices in terms of hole-generation capability of HGL and electron-transporting characteristics of ETL. Specifically, we found that the free hole density in p-doped

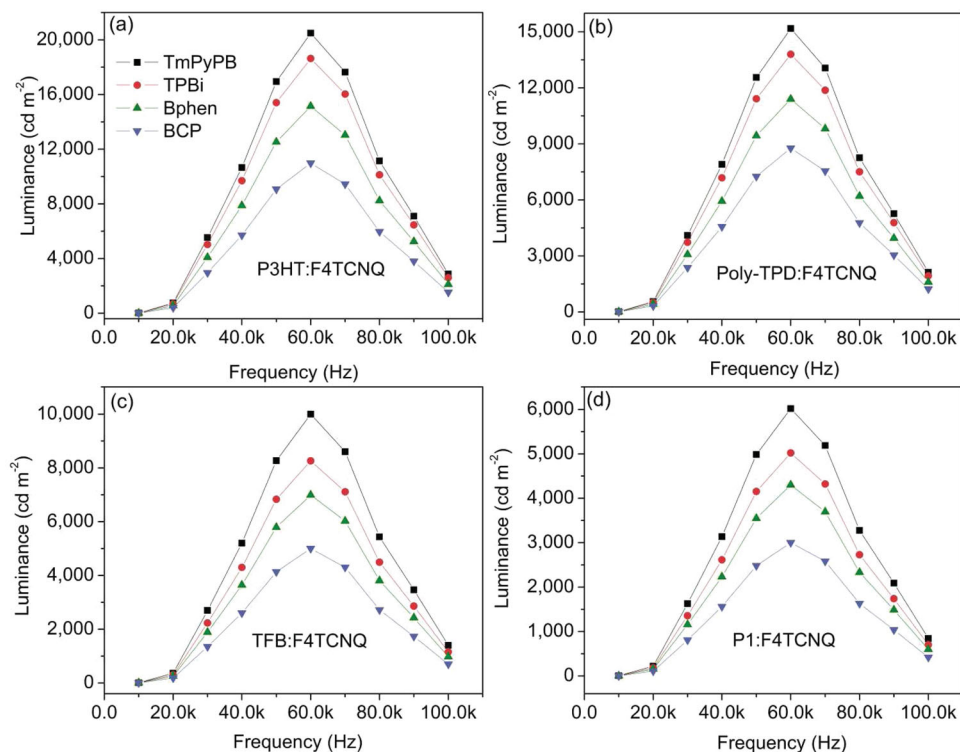


Figure 7. The luminance–frequency characteristics of FIPEL devices with the combination of different HGLs and different ETLs.

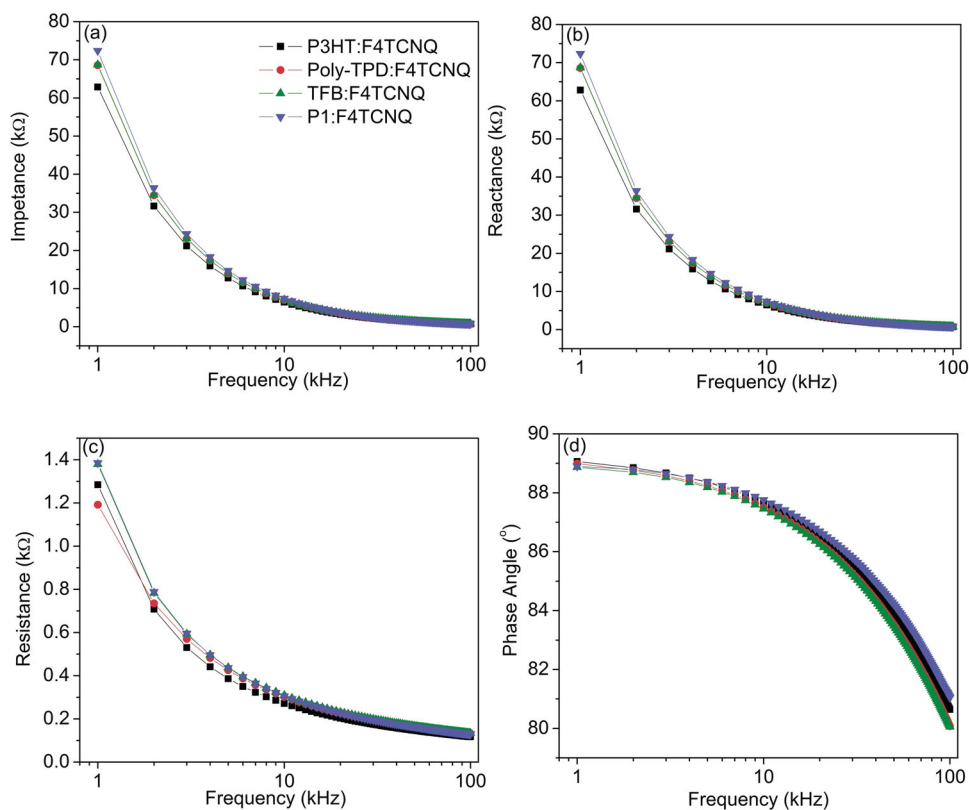


Figure 8. The phase characteristics of FIPEL devices with P3HT:F4TCNQ HGL and TmPyPB ETL. a) Impedance Z , b) reactance X , c) resistance R , and d) phase angle.

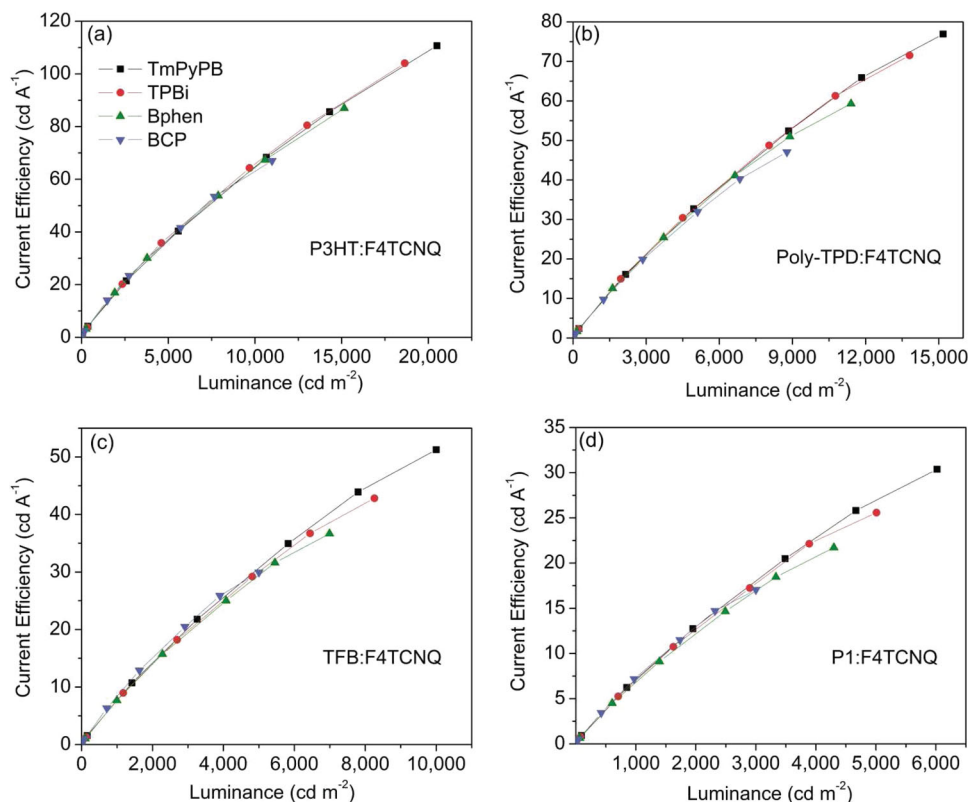


Figure 9. The current efficiencies characteristics as a function of luminance of FIPEL devices with the combination of different HGLs and different ETLs.

HGL and electron mobility of solution-processed ETL are directly related to the device performance. The hole-transporting characteristics of ETLs also play an important role. As a result, our green FIPEL devices with F3HT:F4TCNQ a HGL and TmPyPB as an ETL exhibit exceptional performance: a low turn-on voltage of 12 V, a maximum luminance of 20 500 cd m^{-2} , a maximum current efficiency and power efficiency of 110.7 cd A^{-1} and 29.3 lm W^{-1} . Solution-processed FIPEL devices may well provide an economically attractive alternative to those processed by vacuum deposition, considered essential to low-cost, large area lighting devices. This novel design concept increases the performance of the FIPEL device without significant alteration to its fabrication, perhaps providing a pathway to high performance FIPEL device engineering.

4. Experimental Section

Materials: The high- k relaxor ferroelectric terpolymer dielectrics, poly(vinylidene fluoride-trifluoroethylene-chlorofluoroethylene) [P(VDF-TrFE-CFE)], Poly(N,N' -bis(4-butylphenyl)- N,N' -bis(phenyl)benzidine) (Poly-TPD), and poly(9,9-di- n -octylfluorene-*alt*-(1,4-phenylene-((4-sec-butylphenyl) imino)-1,4-phenylene) (TFB), poly(3-hexylthiophene) (P3HT), and poly(N -vinylcarbazole) (PVK) were purchased from PiezoTech, American Dye Source, and Sigma-Aldrich, respectively. poly[4,8-bis(1-pentylhexyl)benzo[1,2-*b*:4,5-*b'*]dithiophene-2,6-diyl-*alt*-2,1,3-benzoxadiazole-4,7-diyl] (P1) was synthesized by ourselves.^[28] Tetrafluoro-tetracyano-quinodimethane (F4TCNQ), 1,3-bis(2-(4-*tert*-

butylphenyl)-1,3,4-oxadiazole-5-yl)benzene (OXD-7), fac-tris(2-phenylpyridine)iridium(III) [Ir(ppy)₃], 1,3,5-tri(m -pyrid-3-yl-phenyl)benzene (TmPyPB), 1,3,5-Tri(1-phenyl-1H-benzo[d]imidazol-2-yl)phenyl (TPBi), 4,7-diphenyl-1,10-phenanthroline (Bphen), and bathocuproine (BCP) were purchased from Luminescence Technology Corp., Taiwan. All materials were used as received without further purification.

Device Fabrication: All FIPEL devices were fabricated on a glass substrate with a pre-coated ITO film 100 nm thick, with a sheet resistance of approximately 10 Ω/\square . First, the substrates were cleaned in an ultrasonic bath with acetone followed by methanol and isopropanol for 30 min each. The ITO substrates subsequently were dried in a vacuum oven for 2 h and treated with UV-ozone for 20 min. The dielectric layers were made by spin coating 100 mg mL^{-1} P(VDF-TrFE-CFE) solutions in dimethylformamide (DMF) on top of ITO at 1500 rpm inside a nitrogen filled glove box with low moisture and oxygen content (<0.1 ppm), followed by thermal annealing at 135 $^{\circ}\text{C}$ for 4 h. The P3HT (3 mg mL^{-1}), Poly-TPD (10 mg mL^{-1}), TFB (10 mg mL^{-1}), and P1 (2 mg mL^{-1}) doped 7% F4TCNQ as the HGLs in chlorobenzene were spin-coated at 3000 rpm, followed by baking at 120 $^{\circ}\text{C}$ for 30 min. The EML consisted of a blend of PVK and OXD-7 (PVK:OXD-7 = 80:20, wt/wt) as a co-host and 10 wt% Ir(ppy)₃ as the dopant. The EML was obtained by spin coating of the 18 mg mL^{-1} PVK:OXD-7:Ir(ppy)₃ blend in chlorobenzene onto the HGLs at 2000 rpm and dried at 120 $^{\circ}\text{C}$ for 30 min. The 24 mg mL^{-1} small-molecule electron-transport material TmPyPB, TPBi, Bphen, and BCP were dissolved in formic acid:water (FA:H₂O = 3:1) mixture and spun cast onto the EML at a spin speed of 4000 rpm followed by drying at 80 $^{\circ}\text{C}$ for 30 min. Device fabrication was completed by thermal evaporation of LiF (1 nm)/Al (100 nm) electrode through a shadow mask under vacuum at a base pressure of $\approx 5 \times 10^{-6}$ Torr at a rate of 0.05 nm s^{-1} . The thickness of the films was measured by a calibrated Dektak 6M profiler (Veeco). The overlap between ITO and Al electrodes was 3 mm \times 3 mm as the active emissive area of the devices.

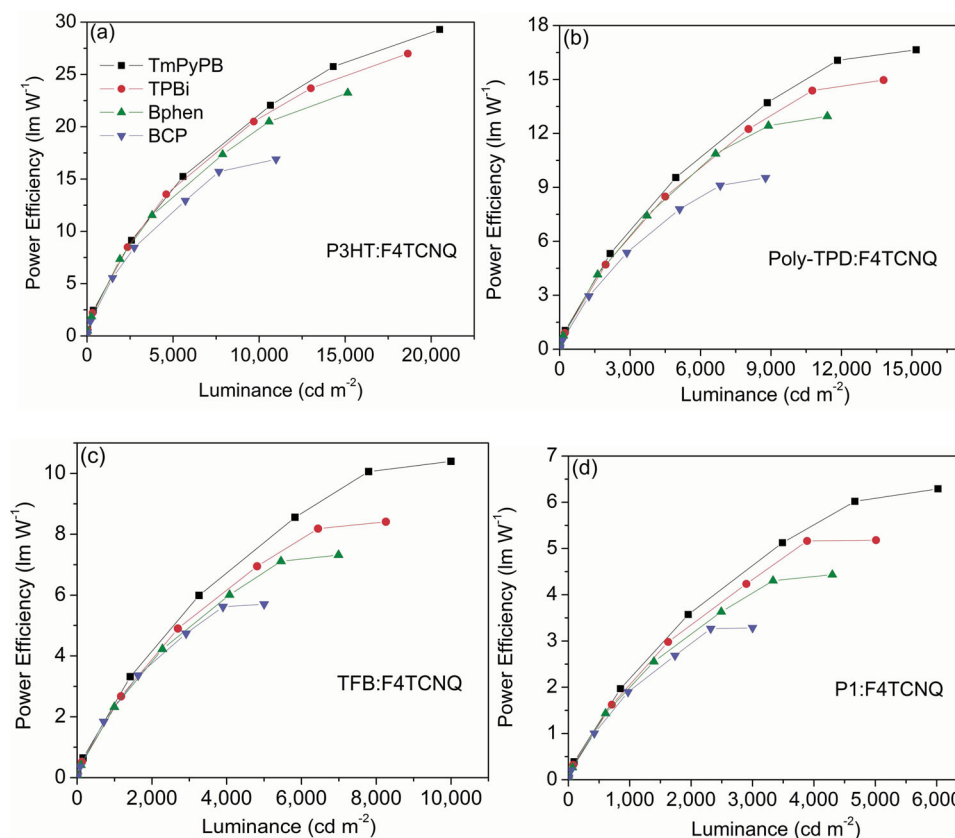


Figure 10. The power efficiencies characteristics as a function of luminance of FIPEL devices with the combination of different HGLs and different ETLs.

Electrical Characterization: The AC sinusoidal voltages were applied from a 200 MHz function/arbitrary waveform generator (Agilent 33220A) connected to a Model PZD700A M/S amplifier (Trek) and the voltage and current was measured on an oscilloscope (Tektronix). The luminance was recorded with an ILT 1400-A photometer (International Light Technologies), as a function of either the AC voltages applied to the devices (at a fixed frequency) or as a function of the frequency of the applied AC voltages (keeping the applied AC voltages constant). The time resolved AC electroluminescence response is detected using a fast photo diode. The phase characteristics are measured with a Keithley 595 quasistatic CV meter. All measurements were carried out under ambient conditions at atmospheric pressure and room temperature.

Acknowledgements

Y.C. and Y.X. contributed equally to this work.

Received: September 19, 2013
Published online: January 16, 2014

- [1] B. W. D'Andrade, S. R. Forrest, *Adv. Mater.* **2004**, *16*, 1585.
- [2] S. Reineke, F. Lindner, G. Schwartz, N. Seidler, K. Walzer, B. Lussem, K. Leo, *Nature* **2009**, *459*, 234.
- [3] B. D'Andrade, *Nat. Photonics* **2007**, *1*, 33.
- [4] F. So, J. Kido, P. Burrows, *MRS Bull.* **2008**, *33*, 663.
- [5] Y. R. Sun, N. C. Giebink, H. Kanno, B. W. Ma, M. E. Thompson, S. R. Forrest, *Nature* **2006**, *440*, 908.

- [6] S. J. Su, E. Gonmori, H. Sasabe, J. Kido, *Adv. Mater.* **2008**, *20*, 4189.
- [7] H. C. Su, H. F. Chen, F. C. Fang, C. C. Liu, C. C. Wu, K. T. Wong, Y. H. Liu, S. M. Peng, *J. Am. Chem. Soc.* **2008**, *130*, 3413.
- [8] Q. B. Pei, Y. Yang, G. Yu, C. Zhang, A. J. Heeger, *J. Am. Chem. Soc.* **1996**, *118*, 3922.
- [9] P. D. Rack, P. H. Holloway, *Mat. Sci. Eng. R* **1998**, *21*, 171.
- [10] J. C. Hitt, J. P. Bender, J. F. Wager, *Crit. Rev. Solid State* **2000**, *25*, 29.
- [11] X. L. Xu, X. H. Chen, Y. B. Hou, Z. Xu, X. H. Yang, S. G. Yin, Z. J. Wang, X. R. Xu, S. P. Lau, B. K. Tay, *Chem. Phys. Lett.* **2000**, *325*, 420.
- [12] S. Y. Yang, L. Qian, F. Teng, Z. Xu, X. R. Xu, *J. Appl. Phys.* **2005**, *97*.
- [13] A. Perumal, M. Frobé, S. Gorantla, T. Gemming, B. Lussem, J. Eckert, K. Leo, *Adv. Funct. Mater.* **2012**, *22*, 210.
- [14] A. Perumal, B. Lussem, K. Leo, *Appl. Phys. Lett.* **2012**, *100*, 103307.
- [15] A. Perumal, B. Lussem, K. Leo, *Org. Electron* **2012**, *13*, 1589.
- [16] J. Sung, Y. S. Choi, S. J. Kang, S. H. Cho, T. W. Lee, C. Park, *Nano. Lett.* **2011**, *11*, 966.
- [17] M. Frobé, A. Perumal, T. Schwab, M. C. Gather, B. Lussem, K. Leo, *Org. Electron* **2013**, *14*, 809.
- [18] Y. H. Chen, G. M. Smith, E. Loughman, Y. Li, W. Y. Nie, D. L. Carroll, *Org. Electron* **2013**, *14*, 8.
- [19] Y. H. Chen, Y. D. Xia, Y. Gu, C. L. Yang, G. M. Smith, D. L. Carroll, *Appl. Phys. Lett.* **2013**, *102*, 013307.
- [20] S. H. Cho, J. Sung, I. Hwang, R. H. Kim, Y. S. Choi, S. S. Jo, T. W. Lee, C. Park, *Adv. Mater.* **2012**, *24*, 4540.
- [21] Y. H. Chen, Y. D. Xia, H. D. Sun, G. M. Smith, D. Z. Yang, D. G. Ma, D. L. Carroll, *Adv. Funct. Mater.* **2013**, DOI: 10.1002/adfm.201302587.
- [22] Y. D. Xia, Y. H. Chen, G. M. Smith, Y. Li, W. X. Huang, D. L. Carroll, *Appl. Phys. Lett.* **2013**, *102*, 253302.

- [23] M. Fröbel, A. Perumal, T. Schwab, C. Fuchs, K. Leo, M. C. Gather, *Phys. Status Solidi A* **2013**, 210, 2439.
- [24] W. Y. Nie, C. M. MacNeill, Y. Li, R. E. Nofle, D. L. Carroll, R. C. Coffin, *Macromol. Rapid. Comm.* **2011**, 32, 1163.
- [25] J. Y. Kim, K. Lee, N. E. Coates, D. Moses, T. Q. Nguyen, M. Dante, A. J. Heeger, *Science* **2007**, 317, 222.
- [26] K. H. Yim, G. L. Whiting, C. E. Murphy, J. J. M. Halls, J. H. Burroughes, R. H. Friend, J. S. Kim, *Adv. Mater.* **2008**, 20, 3319.
- [27] Y. Zhang, B. de Boer, P. W. M. Blom, *Adv. Funct. Mater.* **2009**, 19, 1901.
- [28] L. L. Chua, J. Zaumseil, J. F. Chang, E. C. W. Ou, P. K. H. Ho, H. Sirringhaus, R. H. Friend, *Nature* **2005**, 434, 194.
- [29] P. W. M. Blom, M. J. M. deJong, J. J. M. Vleggaar, *Appl. Phys. Lett.* **1996**, 68, 3308.
- [30] M. A. Lampert, P. Mark, *Current Injection in Solids*, Academic, New York **1970**.
- [31] Q. J. Sun, D. W. Chang, L. I. Dai, J. Grote, R. Naik, *Appl Phys Lett* **2008**, 92.
- [32] S. A. Choulis, V. E. Choong, A. Patwardhan, M. K. Mathai, F. So, *Adv. Funct. Mater.* **2006**, 16, 1075.
- [33] Y. H. Chen, H. K. Tian, Y. H. Geng, J. S. Chen, D. G. Ma, D. H. Yan, L. X. Wang, *J. Mater. Chem.* **2011**, 21, 15332.
- [34] T. Earmme, S. A. Jenekhe, *Adv. Funct. Mater.* **2012**, 22, 5126.
- [35] E. Ahmed, T. Earmme, S. A. Jenekhe, *Adv. Funct. Mater.* **2011**, 21, 3889.
- [36] T. Earmme, E. Ahmed, S. A. Jenekhe, *Adv. Mater.* **2010**, 22, 4744.
- [37] T. Earmme, S. A. Jenekhe, *J. Mater. Chem.* **2012**, 22, 4660.
- [38] V. Coropceanu, J. Cornil, D. A. da Silva, Y. Olivier, R. Silbey, J. L. Bredas, *Chem. Rev.* **2007**, 107, 926.
- [39] H. C. F. Martens, P. W. M. Blom, H. F. M. Schoo, *Phys. Rev. B* **2000**, 61, 7489.
- [40] G. Schwartz, S. Reineke, T. C. Rosenow, K. Walzer, K. Leo, *Adv. Funct. Mater.* **2009**, 19, 1319.
- [41] H. B. Wu, G. J. Zhou, J. H. Zou, C. L. Ho, W. Y. Wong, W. Yang, J. B. Peng, Y. Cao, *Adv. Mater.* **2009**, 21, 4181.
- [42] F. Huang, P. I. Shih, C. F. Shu, Y. Chi, A. K. Y. Jen, *Adv. Mater.* **2009**, 21, 361.
- [43] Y. Zhang, F. Huang, Y. Chi, A. K. Y. Jen, *Adv. Mater.* **2008**, 20, 1565.
- [44] Y. H. Xu, R. Q. Yang, J. B. Peng, A. A. Mikhailovsky, Y. Cao, T. Q. Nguyen, G. C. Bazan, *Adv. Mater.* **2009**, 21, 584.
- [45] X. H. Yang, D. C. Muller, D. Neher, K. Meerholz, *Adv. Mater.* **2006**, 18, 948.
- [46] A. Nakamura, T. Tada, M. Mizukami, S. Yagyu, *Appl. Phys. Lett.* **2004**, 84, 130.
- [47] S. L. Gong, Y. H. Chen, X. Zhang, P. J. Cai, C. Zhong, D. G. Ma, J. G. Qin, C. L. Yang, *J. Mater. Chem.* **2011**, 21, 11197.
- [48] Z. Q. Jiang, Y. H. Chen, C. Fan, C. L. Yang, Q. Wang, Y. T. Tao, Z. Q. Zhang, J. G. Qin, D. G. Ma, *Chem. Commun.* **2009**, 3398.
- [49] C. M. Han, Z. S. Zhang, H. Xu, S. Z. Yue, J. Li, P. R. Yan, Z. P. Deng, Y. Zhao, P. F. Yan, S. Y. Liu, *J. Am. Chem. Soc.* **2012**, 134, 19179.
- [50] L. H. Liu, B. H. Zhang, Z. Y. Xie, J. Q. Ding, L. X. Wang, *Org. Electron.* **2013**, 14, 55.
- [51] Q. Wang, J. Q. Ding, D. G. Ma, Y. X. Cheng, L. X. Wang, F. S. Wang, *Adv. Mater.* **2009**, 21, 2944.
- [52] Q. Wang, J. Q. Ding, D. G. Ma, Y. X. Cheng, L. X. Wang, X. B. Jing, F. S. Wang, *Adv. Funct. Mater.* **2009**, 19, 84.